Acta Crystallographica Section D
Biological Crystallography
ISSN 0907-4449
Editors: **E. N. Baker and Z. Dauter**

Structures of an active-site mutant of a plant 1,3-β-glucanase in complex with oligosaccharide products of hydrolysis

Agnieszka Wojtkowiak, Kamil Witek, Jacek Hennig and Mariusz Jaskolski

Acta Cryst. (2013). D**69**, 52–62

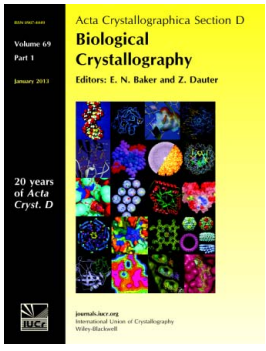

Acta Crystallographica Section D: Biological Crystallography welcomes the submission of papers covering any aspect of structural biology, with a particular emphasis on the structures of biological macromolecules and the methods used to determine them. Reports on new protein structures are particularly encouraged, as are structure–function papers that could include crystallographic binding studies, or structural analysis of mutants or other modified forms of a known protein structure. The key criterion is that such papers should present new insights into biology, chemistry or structure. Papers on crystallographic methods should be oriented towards biological crystallography, and may include new approaches to any aspect of structure determination or analysis. Papers on the crystallization of biological molecules will be accepted providing that these focus on new methods or other features that are of general importance or applicability.

Acta Crystallographica Section D
Biological Crystallography
ISSN 0907-4449

Structures of an active-site mutant of a plant 1,3-β-glucanase in complex with oligosaccharide products of hydrolysis

Agnieszka Wojtkowiak,[a] Kamil Witek,[b] Jacek Hennig[b] and Mariusz Jaskolski[a,c]*

[a]Department of Crystallography, Faculty of Chemistry, A. Mickiewicz University, Poznan, Poland, [b]Institute of Biochemistry and Biophysics, Polish Academy of Sciences, Warsaw, Poland, and [c]Center for Biocrystallographic Research, Institute of Bioorganic Chemistry, Polish Academy of Sciences, Poznan, Poland

Correspondence e-mail: mariuszj@amu.edu.pl

Received 8 September 2012
Accepted 8 October 2012

PDB References: potato endo-1,3-β-glucanase, complex with laminaratriose, 4gzi; complex with laminaratriose and laminaratetrose, 4gzj

Plant endo-1,3-β-glucanases are involved in important physiological processes such as defence mechanisms, cell division and flowering. They hydrolyze (1→3)-β-glucans, with very limited activity towards mixed (1→3,1→4)-β-glucans and branched (1→3,1→6)-β-glucans. Here, crystal structures of the potato (*Solanum tuberosum*) endo-1,3-β-glucanase GLUB20-2 with the nucleophilic Glu259 residue substituted by alanine (E259A) are reported. Despite this active-site mutation, the protein retained residual endoglucanase activity and when incubated in the crystallization buffer with a linear hexameric substrate derived from (1→3)-β-glucan (laminarahexose) cleaved it in two different ways, generating trisaccharides and tetrasaccharides, as confirmed by mass spectrometry. The trisaccharide (laminaratriose) shows higher binding affinity and was found to fully occupy the −1, −2 and −3 sites of the active-site cleft, even at a low molar excess of the substrate. At elevated substrate concentration the tetrasaccharide molecule (laminaratetrose) also occupies the active site, spanning the opposite sites +1, +2, +3 and +4 of the cleft. These are the first crystal structures of a plant glycoside hydrolase family 17 (GH17) member to reveal the protein–saccharide interactions and were determined at resolutions of 1.68 and 1.55 Å, respectively. The geometry of the active-site cleft clearly precludes any (1→4)-β-glucan topology at the subsites from −3 to +4 and could possibly accommodate β-1,6-branching only at subsites +1 and +2. The glucose units at subsites −1 and −2 interact with highly conserved protein residues. In contrast, subsites −3, +3 and +4 are variable, suggesting that the mode of glucose binding at these sites may vary between different plant endo-1,3-β-glucanases. Low substrate affinity is observed at subsites +1 and +2, as manifested by disorder of the glycosyl units there.

1. Introduction

Carbohydrates are the most abundant and widespread organic compounds in nature. The enormous structural diversity of this class of compounds arises from the stereochemical variations of monosaccharides with the same molecular formula and from the different fashions in which monosaccharides can assemble into oligosaccharides and polysaccharides. Carbohydrate-processing enzymes must somehow meet, and overcome, the challenge of selective recognition and turnover of their substrates. Enzymes that hydrolyze the glycosidic bond have been grouped into over 120 families according to an amino-acid sequence-based classification (the Carbohydrate-Active Enzymes database; CAZy; http://www.cazy.org/; Cantarel *et al.*, 2009). The highly specific endo-1,3-β-glucanases (EC 3.2.1.39) catalyze the hydrolysis of β-1,3-glucosidic linkages flanked on each side by segments

consisting of several β-1,3-linked glucosyl residues (Witek *et al.*, 2008) and show only very limited activity towards mixed (1→3,1→4)-β-glucans and branched (1→3,1→6)-β-glucans (Akiyama *et al.*, 1997; Peumans *et al.*, 2000). At high substrate concentrations the reverse transglycosylation reactions are possible (Hrmova *et al.*, 2002), leading to the generation of longer oligosaccharides. The major products of the hydrolysis reactions catalyzed by endo-1,3-β-glucanases are trisaccharides and tetrasaccharides (Moore & Stone, 1972; Keen & Yoshikawa, 1983; Hrmova & Fincher, 1993).

Endo-1,3-β-glucanases have been well characterized in bacteria, fungi and plants. The bacterial enzymes represent two different glycoside hydrolase families, designated GH16 and GH64, which have distinct unrelated folds, namely a β-sandwich jelly roll (Fibriansah *et al.*, 2007) and a two-domain structure consisting of a β-barrel and a mixed α/β domain (Wu *et al.*, 2009). Fungal endo-1,3-β-glucanases belong to family GH55, with a ribcage-like overall architecture formed by two domains with a right-handed parallel β-helix fold (Ishida *et al.*, 2009). The plant enzymes, which are classified as members of the GH17 family, adopt a $(\beta/\alpha)_8$ TIM-barrel fold (Varghese *et al.*, 1994).

Crystallographic studies of plant endo-1,3-β-glucanases have revealed that the proteins possess an ellipsoidal shape, with the catalytic apparatus located at the bottom of a characteristic deep canyon running across the upper part of the molecule. Such an architecture of the substrate-binding cleft allows an endo type of hydrolytic action on long chains of oligosaccharides and/or polysaccharides (Varghese *et al.*, 1994). The major axis of the ellipsoid points at the β2–α2 loop and helix α6 of the TIM barrel and coincides with the general direction of the catalytic groove (Fig. 1). The catalytic residues are placed approximately one-third of the canyon length from its end at loop β2–α2. The groove is extended beyond helix α6

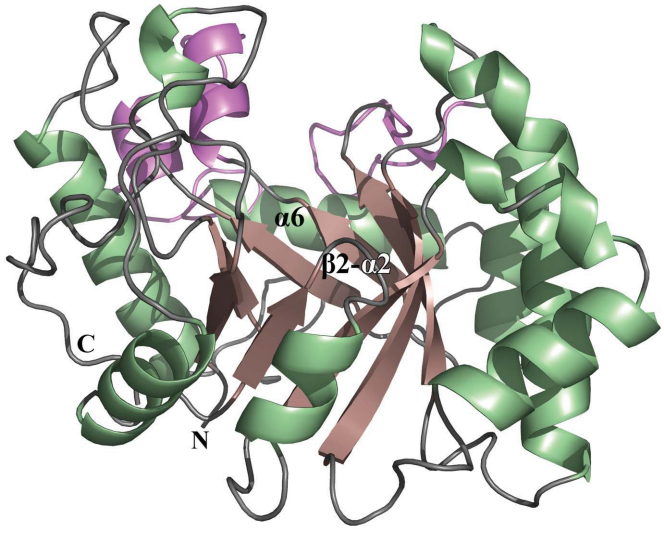

Figure 1
A side view of the overall fold of the E259A mutant of potato endo-1,3-β-glucanase, emphasizing the catalytic cleft on the upper side of the molecule. The strands of the inner β-barrel (red) are surrounded by α-helices (green). The subdomain region (magenta) extends beyond helix α6.

by the presence of a subdomain. The subdomain region of plant endo-1,3-β-glucanases demonstrates high sequence variability and differences in the arrangement of the secondary-structure elements (Wojtkowiak *et al.*, 2012). Extensive studies of the barley isozymes showed that there are eight subsites that accommodate glucosyl residues inside the catalytic cleft (Hrmova *et al.*, 1995). The linear (1→3)-β-D-glucan substrate occupies subsites −3 to +5, with the scissile bond located between residues −1 and +1 (Davies *et al.*, 1997). The binding affinities calculated for the individual subsites of the barley enzyme have the highest values at subsites −2, +4 and +5 (Hrmova *et al.*, 1995), but need not be applicable to other GH17 family members.

As members of the GH17 family, plant endo-1,3-β-glucanases belong to the GH-A clan of glycoside hydrolases. All enzymes of the GH-A clan have a TIM-barrel fold and a conserved catalytic mechanism. The active site consists of two glutamate residues located at the carboxy-termini of β-strands 4 and 7, which act as the proton donor and the nucleophile, respectively (Jenkins *et al.*, 1995; Henrissat *et al.*, 1995). The cleavage reaction yields products that retain the configuration at the anomeric carbon. As expected for retaining enzymes, the distance between the carboxyl and carboxylate groups of the catalytic residues is approximately 5 Å. During the course of hydrolysis, the proton donor protonates the glycosidic O atom of the scissile bond to facilitate the departure of the leaving group. Simultaneously, the nucleophile attacks the anomeric C atom, leading to the formation of a covalent glycosyl-enzyme intermediate. The intermediate is subsequently hydrolyzed by a water molecule. The reaction involves an oxocarbenium-ion transition state with partial double-bond character of the O5—C1 bond. This requires the atoms C2, C1, O5 and C5 to be coplanar, which is achived by half-chair ($^4H_3$, $^3H_4$), boat ($B_{2,5}$, $^{2,5}B$) or envelope (^3E, ^4E) conformations of the pyranoside rings (Fig. 2; Davies *et al.*, 2012).

Endo-1,3-β-glucanases in plants are believed to function as part of a defence mechanism against fungi by hydrolyzing the fungal cell wall, which is built mostly of (1→3)-β-D-glucans. Accordingly, these enzymes are also classified as plant pathogenesis-related class-2 (PR-2) proteins (van Loon *et al.*, 1994). In normal plant growth conditions, they play specialized roles in turnover of callose, cell division, pollen development, seed germination and flowering. Endo-1,3-β-glucanases have been identified as allergens in pollen grains (Huecas *et al.*, 2001), natural rubber latex (Sunderasan *et al.*, 1995) and fresh fruits (Wagner *et al.*, 2004).

Despite extensive studies of plant endo-1,3-β-glucanases, no structural information has been reported to date on their mode of interaction with oligosaccharide ligands. In this study, Glu259, the catalytic nucleophile of endo-1,3-β-glucanase from *Solanum tuberosum* (GLUB20-2), was mutated to alanine. Subsequently, the E259A GLUB20-2 mutant protein was cocrystallized with a hexasaccharide derived from (1→3)-β-D-glucan (laminarahexose) in order to map the atomic interactions between the protein and its substrate. The substrate turned out to be enzymatically hydrolyzed into two trisaccharides or to a disaccharide and a tetrasaccharide

despite the crippling E259A mutation of the enzyme. The products of this reaction, a trisaccharide or a trisaccharide and tetrasaccharide pair, formed complexes with the protein and their structures have been determined at high resolution and are presented in this work. We are thus able to provide, for the first time, a detailed description at the atomic level of the interactions of the protein with an oligosaccharide ligand at its substrate-binding subsites.

2. Materials and methods

2.1. Cloning, expression and purification

cDNA coding for the endo-1,3-β-glucanase from *S. tuberosum* was amplified by PCR using the *gluB20-2* ORF and cloned into pTOPO vector as described previously (Wojtkowiak *et al.*, 2012). The E259A replacement was introduced into the coding sequence of *gluB20-2* by site-directed mutagenesis following protocols described by Green & Sambrook (2012), with the use of forward (GTATCG**GCA**AGTGGTTGGCCTTCTGAGGGACA) and reverse (GGTGTCCCTCAGAAGGCCAACCACT**TGC**CGAT) primers coding for the mutation (bold). The mutant cDNA was cloned into pET30a vector and sequenced. The recombinant gene was expressed in *Escherichia coli* BL21 strain (Studier & Moffatt, 1986) using TB medium (Green & Sambrook, 2012). The bacterial culture was incubated at 310 K until its optical density reached A_{600} = 1. Protein synthesis was induced by the addition of isopropyl β-D-1-thiogalactopyranoside (IPTG) to a final concentration of 0.25 m*M* and incubation was continued at 291 K for 24 h. Finally, the culture was centrifuged at 8000*g* at room temperature for 10 min. The bacterial cells were collected and kept overnight at 253 K. Protein purification was performed as described by Wojtkowiak *et al.* (2012). The homogenous protein fractions were pooled together, dialyzed against 25 m*M* sodium phosphate buffer pH 7.8 with the addition of 10%(*v*/*v*) glycerol and kept as 1 mg aliquots at 253 K. For crystallization experiments, the protein was concentrated to 7 mg ml^{-1} and the buffer was exchanged to 20 m*M* Tris–HCl pH 8.0 using Millipore Centricon 10 filters.

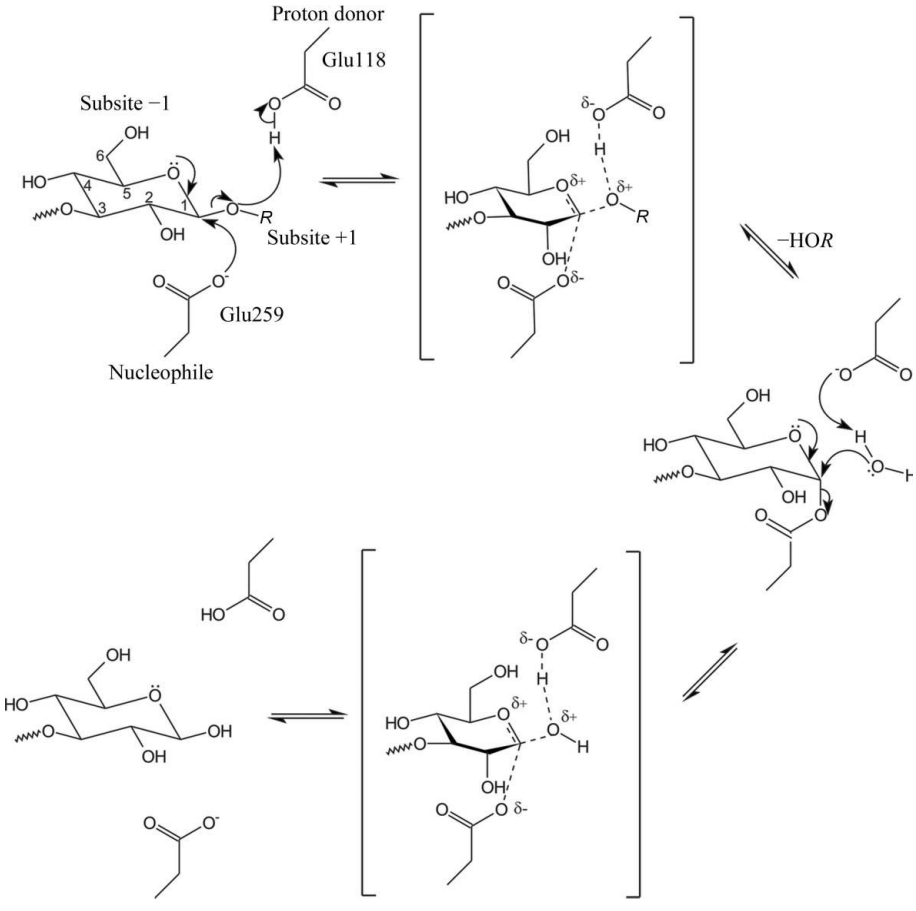

Figure 2
Schematic mechanism of the reaction catalyzed by endo-1,3-β-glucanase according to Davies *et al.* (1998).

2.2. Crystallization

Prior to crystallization experiments, the E259A mutant of recombinant potato endo-1,3-β-glucanase was incubated for 3 h at 277 K with either a hexameric or a pentameric linear (1→3)-β-glucan oligosaccharide. The hexasaccharides and pentasaccharides, which were derived from longer (1→3)-β-glucan polymers and isolated as high-purity samples, were a kind gift from Professor Tadeusz Antczak (Technical University of Lodz). Sparse-matrix screening (Structure Screen 1 and 2; Molecular Dimensions Ltd) for crystallization conditions of a pentasaccharide complex was not successful, whereas the incubation mixture with the hexasaccharide yielded crystals of two different complexes with the protein. In one case (3G) crystals were obtained with a threefold molar excess of the oligosaccharide and in the other case (7G) with a sixfold molar excess of the ligand. Crystals of both complexes were obtained by vapour diffusion at 292 K in hanging drops made up of 1.5 µl protein/ligand solution and 1.5 µl reservoir solution consisting of 0.1 *M* sodium citrate pH 5.6, 0.2 *M* ammonium acetate, 24% PEG 8000. Crystals grew over a period of 2–7 d in the form of bunched needles. Single and larger crystals were obtained by the use of streak-seeding and were left in the crystallization drops until data collection (two months).

2.3. Data collection and processing

X-ray diffraction data for both complexes were collected on beamline X11 at the EMBL Hamburg with 0.5° oscillation and 1.68 Å resolution for the 3G complex and with 0.75° oscillation

Table 1
X-ray data-collection and refinement statistics.

Values in parentheses are for the highest resolution shell.

	3G	7G
Data collection		
Radiation source	X11, EMBL Hamburg	X11, EMBL Hamburg
Wavelength (Å)	0.81620	0.81480
Temperature of measurements (K)	100	100
Space group	$P2_1$	$P2_1$
Unit-cell parameters (Å, °)	a = 54.9, b = 49.3, c = 57.1, β = 98.4	a = 55.3, b = 49.2, c = 57.4, β = 98.8
Mosaicity (°)	0.781	0.488
Protein molecules in asymmetric unit	1	1
Solvent content (%)	41	42
Resolution range (Å)	30.00–1.68 (1.74–1.68)	40.00–1.55 (1.61–1.55)
No. of unique reflections	34231	44391
$R_{\rm merge}$†	0.069 (0.264)	0.091 (0.680)
Completeness (%)	99.0 (92.7)	100.0 (100.0)
$\langle I/\sigma(I)\rangle$	23.2 (5.1)	15.3 (2.1)
Multiplicity	6.2 (4.8)	3.8 (3.8)
Refinement statistics		
Resolution (Å)	20.0–1.68	20.0–1.55
No. of reflections	34202	44352
No. of reflections in test set	1076	1139
$R_{\rm work}$‡	0.136	0.151
$R_{\rm free}$	0.171	0.181
No. of residues	315	315
No. of non-H atoms		
Protein	2524	2528
Ligand	34	57
Water molecules	338	356
R.m.s.d. from ideal bond lengths (Å)	0.017	0.017
R.m.s.d. from ideal bond angles (°)	1.57	1.64
Average B factors (Å^2)	17.5	15.3
Ramachandran statistics (%)		
Most favoured regions	91.1	90.4
Additionally allowed regions	8.9	9.6
PDB code	4gzi	4gzj

† $R_{\rm merge} = \sum_{hkl}\sum_i |I_i(hkl) - \langle I(hkl)\rangle|/\sum_{hkl}\sum_i I_i(hkl)$, where $I_i(hkl)$ is the intensity of observation i of reflection hkl. ‡ $R_{\rm work} = \sum_{hkl} ||F_{\rm obs}| - |F_{\rm calc}||/\sum_{hkl}|F_{\rm obs}|$ for reflections in the working set, where $F_{\rm obs}$ and $F_{\rm calc}$ are the observed and calculated structure factors, respectively. $R_{\rm free}$ is calculated analogously for test reflections randomly selected and excluded from the refinement.

and 1.55 Å resolution for the 7G complex. The data collection was performed at 100 K with the use of 40%(*v*/*v*) PEG 400 mixed in a 1:1(*v*:*v*) ratio with the reservoir solution as a cryoprotectant. The data were indexed, integrated and scaled with *HKL*-2000 (Otwinowski & Minor, 1997). In both cases the crystals were monoclinic, belonging to space group $P2_1$, and the asymmetric unit contained one protein molecule. A summary of the data-collection and processing statistics is given in Table 1.

2.4. Structure determination and refinement

The structure of the 3G complex was determined by molecular replacement using the coordinates of native potato endo-1,3-β-glucanase (PDB entry 3ur7, molecule *A*; Wojtkowiak *et al.*, 2012) as a search model. The rotational and translational searches were performed with the *MOLREP* program (Vagin & Teplyakov, 2010). Structural refinement was carried out in *REFMAC*5 (Murshudov *et al.*, 2011) using maximum-likelihood targets. Manual adjustments of the model in electron-density maps were performed in the *XtalView* program (McRee, 1999). For TLS analysis of the protein model, the *TLSMD* server was used (Painter & Merritt, 2006) and three TLS segments were defined per polypeptide chain. When the refinement reached R and $R_{\rm free}$ values of 0.243 and 0.276, respectively, a difference map was calculated, which unambiguously showed a trisaccharide (laminaratriose) molecule docked in one-half of the binding cleft. The ligand molecule was built manually according to the electron density with the aid of the *PRODRG* server (Schüttelkopf & van Aalten, 2004). In the final stages of modelling water molecules were added to the coordinate set and the refinement converged at R and $R_{\rm free}$ values of 0.136 and 0.171, respectively, with the use of all reflections to the full resolution of 1.68 Å. The 3G structure was subsequently used for the determination of the structure of the 7G complex. All structure-determination and refinement steps for the 7G complex were as for the 3G complex, except that the difference electron-density maps showed not only the same trisaccharide as before but also another oligosaccharide bound in the second half of the catalytic cleft. From the space spanned by this ligand it is obvious that it consists of four glucose units (laminaratetrose), but only two of them (at subsites +3 and +4) could be built in electron-density maps without ambiguity. The refinement of the 7G structure converged at R and $R_{\rm free}$ values of 0.151 and 0.181, respectively, for all reflections to the full resolution of 1.55 Å. A summary of the refinement statistics is given in Table 1. Structural superpositions were calculated using *ALIGN* (Cohen, 1997). Molecular and electron-density illustrations were prepared in *PyMOL* v.1.3 (Schrödinger LLC).

2.5. Mass-spectrometry experiments

The molecular masses of the oligosaccharides were determinated using a Kratos Kompact-SEQ MALDI-TOF mass spectrometer. Prior to analysis, the samples were purified by the use of Dowex 50WX8 ion-exchange resin. The molecular masses were estimated from the m/z ratio of the ionic adducts (M + Na^+). 2,5-Dihydroxybenzoic acid and 2′,4′,6′-trihydroxyacetophenone were used as a matrix.

3. Results and discussion

3.1. Overall structures

Crystalline complexes of E259A GLUB20-2 with oligosaccharides were obtained by cocrystallization. For the cocrystallization experiments, a pentasaccharide or a hexasaccharide derived from (1→3)-β-glucan (laminaran) were used as potential ligands. In the case of the pentasaccharide, all crystallization trials failed. In contrast, in the case of the hexasaccharide ligand two different complexes were crystallized. In one case, which was obtained with a lower protein: hexasaccharide molar ratio (1:3), the protein subsites −1 to −3 were occupied by a trisaccharide (laminaratriose). In the other crystal, which was grown at a higher molar excess of the ligand (1:6), in addition to the trisaccharide found in exactly the same place an additional tetrasaccharide (laminaratetrose) was bound at subsites +1 to +4. The tetrasaccharide was less perfectly bound in its binding site and only the glucose units at subsites +3 and +4 were included in the model (at full occupancy). However, the distinct electron density that extends from subsite +3 towards the catalytic centre (especially at +1) was interpreted as indicating that a tetrasaccharide was present at this site. Indeed, the available space is perfectly compatible with four glucose units and a provisionally docked tetrasaccharide at this site would have its nonreducing end within 2.9 Å of the reducing end of the fully modelled trisaccharide. Moreover, the presence of a tetrasaccharide was confirmed experimentally by mass-spectrometric analysis of an incubation buffer that simulated the crystallization conditions (see below). However, because of the evident disorder at subsites +1 and +2, the tetrasaccharide model included in the coordinate set is limited to residues +3 and +4 which could be modelled with confidence. According to the number of occupied subsites, the complex structures are denoted as 3G and 7G in the following.

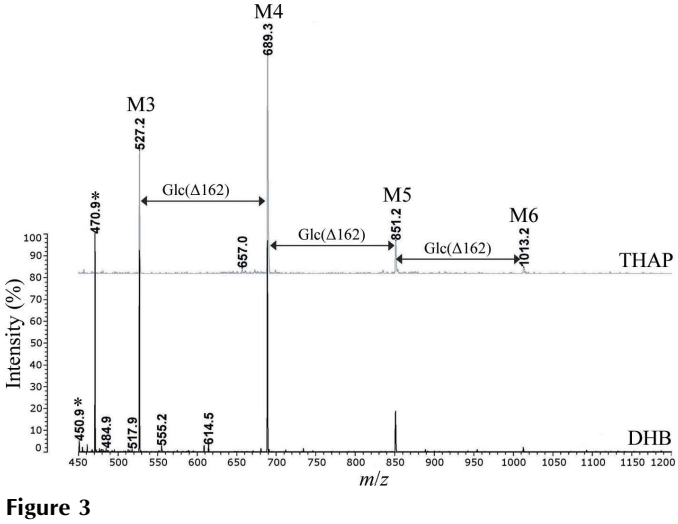

Figure 3
MALDI-TOF ionization mass-spectrometric analysis of the hydrolysis products of a hexasaccharide (1→3)-β-glucan catalyzed by the E259A mutant of GLUB20-2. M6, M5, M4 and M3, molecular masses of ionic adducts of Na^+ and hexasaccharides, pentasaccharides, tetrasaccharides and trisaccharides, respectively; *, matrix ions (DHB, 2,5-dihydroxybenzoic acid; THAP, 2′,4′,6′-trihydroxyacetophenone).

Both complexes crystallized in space group $P2_1$ with one protein molecule in the asymmetric unit and with very similar unit-cell parameters (Table 1). The 3G and 7G crystal structures were determined by molecular replacement and refined to 1.68 and 1.55 Å resolution, respectively, with good refinement statistics (Table 1). The models of both structures contained all 315 amino-acid residues of the mature protein (residues 24–338). The C-terminal histidine tag (residues 339–346) could not be modelled owing to disorder. It is interesting to note that in the crystal structures of the ligand-free native protein reported previously the His tag was docked into the active site of an adjacent protein molecule, linking them into infinite linear chains (Wojtkowiak *et al.*, 2012).

The trisaccharide molecule is docked at the −1, −2 and −3 subsites, with its nonreducing terminus at the far end of the binding cleft (−3) marked by the β2–α2 loop of the protein. The tetrasaccharide is bound at the plus-numbered subsites with its reducing terminus at the other end of the binding cleft (+4) near helix α6. In this binding mode, the reducing end at subsite −1 and the nonreducing end at subsite +1 meet at the catalytic centre, showing the pattern of products of the hydrolytic reaction catalyzed by the enzyme. At the same time, the scheme of interactions of the polar groups of the saccharides with the protein residues defines the precise enzyme–substrate recognition pattern in atomic detail.

3.2. Structural comparisons

The protein molecules in both structures are essentially identical, as illustrated by the small r.m.s.d. value (0.12 Å) calculated for all their C^α atoms. The trisaccharide molecules bound in the catalytic clefts of both structures occupy the same position and have an identical conformation, as illustrated by the r.m.s.d. value of 0.09 Å calculated for all of their non-H atoms in a superposition based on the protein C^α atoms only. Superpositions of the present mutant structures with the native protein molecule (molecule *A* from PDB entry 3ur7; Wojtkowiak *et al.*, 2012) also yielded very small r.m.s.d. values for all C^α atoms (0.22 and 0.25 Å for 3G and 7G, respectively), demonstrating an identical overall conformation. The E259A GLUB20-2 molecule has the $(\beta/\alpha)_8$ TIM-barrel fold architecture typical of all plant endo-1,3-β-glucanases. The deep catalytic cleft is located in the upper part of the enzyme, over the C-terminal face of the barrel, and runs across the entire molecule. The side walls of the cleft are built up by the helices and loops. The most flexible region of the structure is the additional subdomain situated around helix α6 (Wojtkowiak *et al.*, 2012). This subdomain, which forms part of the catalytic cleft, consists of loops located around helix α6 (β6–α6 and β5–α5) and of additional secondary-structure elements located within these loops: two short antiparallel β-strands located in the β5–α5 loop and two short α-helices located in loop β6–α6.

3.3. Mass-spectrometric analysis of the hydrolytic products

The oligosaccharides located in the catalytic cleft of both complex structures are shorter than the hexasaccharide used for crystallization and must have arisen by hydrolysis.

Therefore, hydrolysis was catalyzed by the protein despite the mutation of the active-site nucleophile. To confirm these observations, a mass-spectrometric (MS) analysis of the oligosaccharides was perfomed. The sample of the hexamer used in the crystallization trials contained predominantly hexasaccharide and a trace amount of pentasaccharide (data not shown). An MS analysis of oligosaccharides harvested directly from the crystals was unsuccessful, probably owing to the presence of polyethylene glycol or/and an insufficient amount of the target oligosaccharides. Therefore, a test of the hydrolytic activity of the E259A protein mutant was carried out in a separate experiment under conditions identical to the crystallization conditions except for the elimination of the polyethylene glycol component. The sample was analysed after two months of incubation, *i.e.* after a period of time equivalent to the duration of the crystallization experiment up to the point of data collection. As expected, the incubation mixture contained mainly tetrasaccharides (most abundant) and trisaccharides (Fig. 3). To confirm that the hexasaccharide does not undergo spontaneous hydrolysis, an identical test was performed without addition of the enzyme; the MS analysis of the incubation mixture excluded such a possibility (data not shown).

3.4. Hydrolysis-product pattern and binding affinities

The endohydrolytic activity of the GLUB20-2 protein allows processing of the hexasaccharide substrate used in the crystallization experiments into two identical trisaccharide molecules or into a tetrasaccharide and a disaccharide. The production of trisaccharide molecules induced crystallization of the 3G complex, with the trimer bound at the nonreducing (glycon portion) end of the binding cleft. Potential complexes with a disaccharide bound at the glycon site were not formed, probably because in the incubation equilibrium the shorter product was outperformed in binding efficiency by the longer trisaccharide. Kinetic and thermodynamic studies of barley endo-1,3-β-glucanases (Hrmova *et al.*, 1995) show an absence of any significant binding at positions beyond subsite −3, which is consistent with our results. With higher substrate/product concentration, the aglycon portion of the binding cleft is also occupied in crystal 7G. There is crystallographic evidence (disorder) suggesting that in this case the binding at subsites +1 and +2 is weak and that efficient docking is achieved only at the farther subsites (+3 and +4). There is a theoretical possibility that the +1, +2, +3 and +4 subsites in the 7G structure could be occupied by a disaccharide/trisaccharide/tetrasaccharide mixture with (combined) full occupancy only at subsites +3 and +4. However, since endo-glucanases are specific for the recognition and turnover of long saccharide chains, binding of a short oligomer far away (up to 10 Å) from the catalytic centre is not a likely scenario. It is obvious that the two product molecules modelled in the 7G complex could not have arisen in a single hydrolytic act, *i.e.* cleavage and product retention, of the hexasaccharide substrate. It must be thus assumed that the complex formation is a dynamic process that also involves diffusion (out and in) of the hydrolytic products, with the additional possibility of a transglycosylation reaction. Such an interpretation does not invalidate the crystallographic 7G model; on the contrary, it makes it even more useful because the oligosaccharides span seven binding subsites and not just six as would be possible with the original hexasaccharide. The oligosaccharide–enzyme interactions are described in detail in the following sections.

3.5. Protein interactions at the nonreducing end of the oligosaccharide

In both the 3G and 7G structures the trisaccharide molecule is situated in a negatively charged portion of the catalytic cleft and occupies subsites −1 to −3 (glycon portion). The electron density is very well defined, showing that all three glucose units adopt the relaxed chair conformation $^4C_1$ (Fig. 4). The glucose units at subsites −1 and −2 interact with the highly conserved residues Asn117, Glu310, Lys313 and Glu319. There are eight direct protein–ligand hydrogen bonds plus two water-mediated interactions for just these two subsites (Table 2). Asn117 is strictly conserved in clan GH-A enzymes, immediately preceding the catalytic proton donor Glu118 in the sequence. The importance of the amino-acid residues at sites Glu310, Lys313 and Glu319 for the hydrolysis reaction has been confirmed by site-directed mutagenesis studies of barley endo-1,3-β-glucanase (Chen *et al.*, 1995). The presence

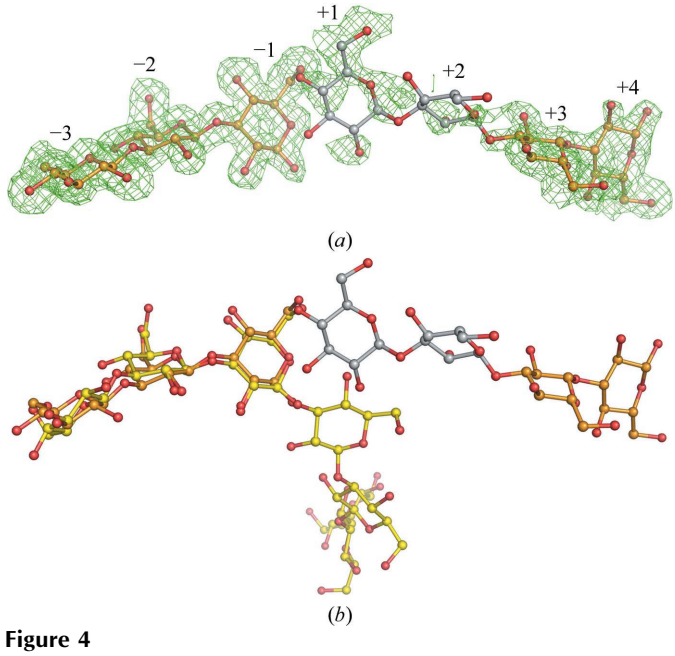

Figure 4
Atomic models of (1→3)-β-glucans. (*a*) The carbohydrate molecules bound in the catalytic cleft of the present 1,3-β-glucanase in the 7G complex. Electron density is shown as an $F_o - F_c$ OMIT map (green) contoured at 2.5σ. The models in orange represent the glucose units built in electron-density maps and included in the coordinate set; the two units of the tetrasaccharide shown in grey (+1 and +2) are not part of the crystallographic model because of disorder and have been tentatively placed in the visible electron density in the binding groove only for the purpose of this figure (and Fig. 7) to illustrate the length and general shape of the ligand in subsites +1 to +4. (*b*) A heptamer modelled by Bohne *et al.* (1999) using *SWEET*2 (yellow) superposed on the nonreducing end of the trisaccharide of the present 7G complex.

Table 2
Hydrogen-bonding and hydrophobic interactions with aromatic side chains between the oligosaccharide ligands and the protein.

Glucose unit at subsite	Direct hydrogen bonds	Water-mediated hydrogen bonds	Hydrophobic interactions with aromatic rings
−3	Gln82 $O^{\varepsilon1}\cdots$O-3	Asn81 N$\cdots$O-2	
	Gln82 $N^{\varepsilon2}\cdots$O-4	Lys32 N$\cdots$O-6	
		His61 $N^{\varepsilon2}\cdots$O-6	
−2	Asn117 $N^{\delta2}\cdots$O-2	Glu11 $O^{\varepsilon1}\cdots$O-2	Tyr58$\cdots\beta$-face†
	Lys313 $N^{\zeta}\cdots$O-5	Lys32 N$\cdots$O-4	
	Lys313 $N^{\zeta}\cdots$O-6		
	Glu310 $O^{\varepsilon1}\cdots$O-6		
−1	Lys313 $N^{\zeta}\cdots$O-4		Phe305$\cdots\beta$-face†
	Glu319 $O^{\varepsilon1}\cdots$O-4		Phe322$\cdots$C-6
	Glu319 $O^{\varepsilon2}\cdots$O-6		
	Tyr201 $O^{\eta}\cdots$O-5		
+3	Thr166 $O^{\gamma1}\cdots$O-6	Tyr201 O$\cdots$O-2	
		Gly161 O$\cdots$O-4	
		Arg175 $N^{\eta}H\cdots$O-4	
+4	Thr166 $O^{\gamma1}\cdots$O-4	Gly205 O$\cdots$O-2	
	Thr166 O$\cdots$O-6	Ser240 $O^{\gamma}\cdots$O-4	

† In the conventional Haworth representation (McNaught & Wilkinson, 1997) of the glucose molecule, the β-face is located beneath the pyranose-ring plane.

of these residues is crucial for efficient catalysis. The enzyme–ligand interactions at the hydrophobic surfaces of the aromatic side chains are the characteristic ligand-recognition patterns found in many glycoside hydrolases. In the present case, the aromatic ring of Tyr58 makes contacts with glucosyl −2 and those of Phe305 and Phe322 make contact with the −1 glucose (Fig. 5). The position of Phe305 in the structure is defined by an unusual *cis*-peptide bond formed with the preceding Ala304. The interactions of hydroxyls O-1 and O-2 of glucose at subsite −1 with Wat259 were not taken into account because the presence of this water molecule is an artificial consequence of the side-chain reduction introduced by the E259A mutation, as described in the next section. The glucosyl residue at the −3 subsite forms three solvent-mediated and two direct interactions with the protein (Table 2). The O-3 and O-4 hydroxyls are directly hydrogen-bonded to the $O^{\varepsilon1}$ and $N^{\varepsilon2}$ atoms of Gln82, respectively. The tight binding and steric clashes around the O-3 hydroxyl group preclude the insertion of another glucosyl moiety at the −4 subsite, thus limiting the glycon product of the reaction to trisaccharides. This provides a plausible explanation of the preferences of this plant endo-1,3-β-glucanase for the trisaccharide products of the hydrolysis reaction. Gln82, which is part of a short flexible 3_{10}-helix preceding the third α-helix of the TIM-barrel fold, is not conserved in other plant endo-1,3-β-glucanases. It is often replaced by serine or aspartate residues. It can therefore be expected that there will be differences between plant endo-1,3-β-glucanases in the binding mode of the glucosyl residue at subsite −3.

3.6. The −1 subsite

The position of the glucose unit at subsite −1 is defined by interactions with strictly conserved residues (Table 2). The hydroxyl groups O-1 and O-2 interact only with Wat259. This situation is not typical for glucoside hydrolases and is a consequence of the mutation of the catalytic nucleophile Glu259 to alanine. The small side chain of the alanine residue allows the hydroxyls O-1 and O-2 of glucose −1 to slip into the empty space left by the glutamate (Fig. 5). A superposition of the complex and the native enzyme structure shows that hydroxyl O-1 would be at a distance of only 1 Å from the $O^{\varepsilon2}$ atom of Glu259. However, the interaction of the nucleophile $O^{\varepsilon1}$ atom with the O-2 hydroxyl of the substrate, which is strictly conserved in clan GH-A, is emulated in the 7G and 3G structures by Wat259, which is additionally hydrogen-bonded to the hydroxyl group of Tyr58 in the same manner as the Glu259 $O^{\varepsilon1}$ atom in the native structure. Another clan GH-A characteristic interaction of glucose residue −1 is a hydrogen bond between the O-2 hydroxyl and the $N^{\delta2}$ atom of the asparagine residue preceding the proton donor (Asn117). In the complex structures of the mutated protein, the $N^{\delta2}$ atom of Asn117 instead interacts with the O-2 hydroxyl of the glucosyl residue at the −2 subsite, but the position of the Asn117 side chain in the mutant and in the native protein is different.

The pyranoside rings in the −1 subsite undergo conformational changes during the hydrolysis reaction, as reviewed by Vocadlo & Davies (2008) and Davies *et al.* (2012). The pathway of the conformational changes typical for retaining β-glycosidases is $^{1}S_{3}\leftrightarrow[^{4}H_{3}]^{\ddagger}\leftrightarrow{}^{4}C_{1}$. To better analyze the interactions at the −1 subsite, the structures of the native and mutated GLUB20-2 protein were superposed and the −1 glucose conformation was changed from $^{4}C_{1}$ to $^{4}H_{3}$ (Fig. 6). With this new conformation docked in the native protein, the hydroxyls O-4, O-3 and the ring O atom O-5 establish exactly the same interactions with the enzyme as found for the chair conformation; in addition, the O-1 hydroxyl interacts with the $O^{\varepsilon2}$ atom of Glu259 and the O-2 hydroxyl interacts with Glu259 $O^{\varepsilon1}$ and Asn117 $N^{\delta2}$, which is typical for the GH-A clan.

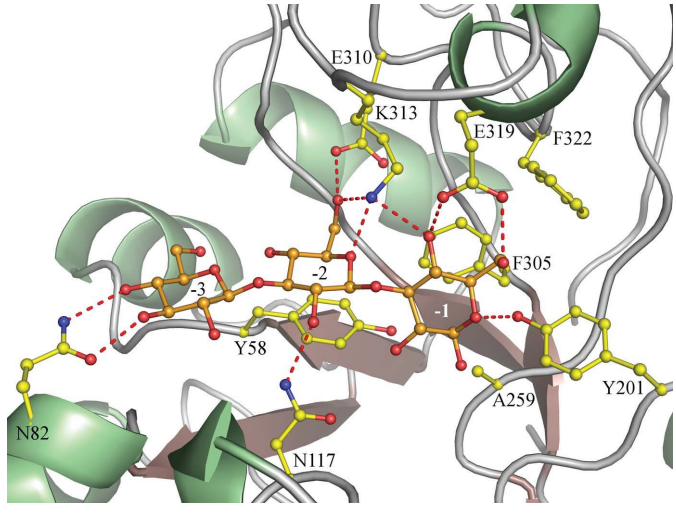

Figure 5
The interactions of the trisaccharide ligand (orange) bound at the −1, −2 and −3 subsites of the protein. The key protein residues are shown in yellow and hydrogen bonds are marked by dashes. Note the site of the Ala259 mutation: the space freed by the side chain of Glu259 was occupied by the sugar unit −1, which is now in a relaxed $^{4}C_{1}$ conformation.

3.7. Consequences of the E259A mutation

In the native structure of GLUB20-2 (PDB entry 3ur7) the $O^{\varepsilon2}$ (catalytic centre) and $O^{\varepsilon1}$ atoms of the catalytic nucleophile Glu259 form hydrogen bonds to Tyr201 O^{η} and to Tyr58 O^{η}, respectively. The proton donor Glu118 and the strictly conserved Asn117 form a hydrogen-bond network with Arg56 and Asn199 which stabilizes their positions in the structure, readying them for interactions with the incoming oligosaccharide (Fig. 7*b*). In the mutant complex structures 3G and 7G the side chain of Asn117 has moved away to form a hydrogen bond to the O-2 hydroxyl of the glucosyl residue at subsite −2, breaking part of the hydrogen-bond network mentioned above (Fig. 7*a*). However, as described previously, in the case of a properly placed glucosyl residue at subsite −1 the hydrogen-bond network will be preserved. The mutation of Glu259 to alanine has created sufficient space to accommodate a water molecule. This water molecule, Wat259, is hydrogen bonded to Tyr58, Arg56 and Asn199.

In many glycosidases, replacement of the catalytic nucleophile by a shorter residue allows small external anions such as azide, formate or halides to effectively cleave the glycosidic bond (Zechel & Withers, 2001). In the present mutant this is not the case since no modified oligosaccharides were detected in the mass-spectrometry experiments. We therefore postulate that the role of a nucleophile could possibly be played by a water molecule accommodated in a fashion similar to Wat259 but hydrogen-bonded to Tyr201 O^{η}, which would place it in the position of Glu259 $O^{\varepsilon2}$. This situation could lead to inversion of the configuration at the anomeric carbon; however, a second water molecule approaching from the opposite direction after the departure of the leaving group would invert the configuration again to the more stable β form before diffusion of the final oligosaccharide product from the enzyme. A water molecule acting as a nucleophile has been observed, for example, in *Micromonospora viridifaciens* sialidase (Watson *et al.*, 2003). There is also a slim possibility that the observed residual activity is the consequence of contamination by trace amounts of the native form introduced during protein purification or by amino-acid misincorporation during protein synthesis (Laughrea *et al.*, 1987; Toth *et al.*, 1988).

3.8. Leaving group–enzyme interactions

During the course of the hydrolytic reaction, the leaving group (aglycon portion, containing the reducing end of the original oligosaccharide substrate) diffuses away from the active centre and is replaced by a water molecule that is used to hydrolyze the glycosyl-enzyme intermediate (Fig. 2). In the 7G complex, the docking interactions anchoring the tetrasaccharide leaving group in the binding cleft are evidently weaker than at the complementary trisaccharide site. The glucosyl residues at the +1 and +2 subsites could not be modelled with reliability owing to their disorder (Fig. 3). Nevertheless, for glucosyl +1 a hydrophobic interaction with Phe204 can be expected. The glucose units at the +3 and +4 subsites form direct hydrogen bonds to a common residue, Thr166 (Table 2). Thr166 is located in the additional subdomain region of the $\beta5$–$\alpha5$ loop (Fig. 8), which is the most

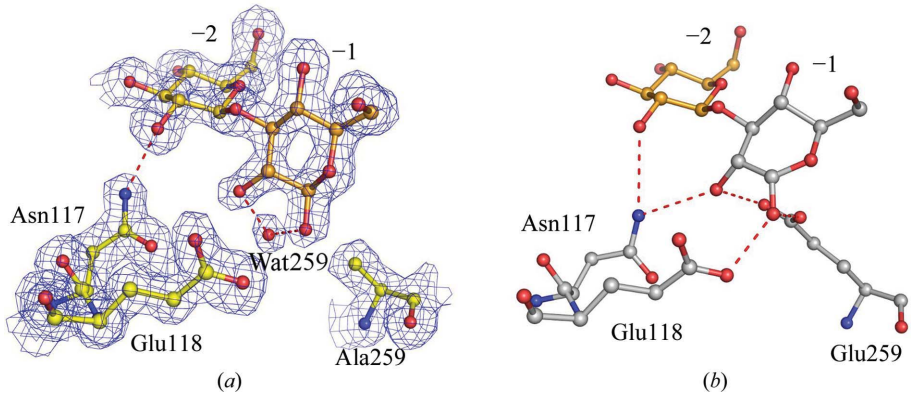

Figure 6
The interactions of the glucose units −2 and −1 with the strictly conserved GH-A clan residues, namely two glutamic acids, the catalytic nucleophile (259, here mutated to alanine) and the proton donor (118), and an asparagine (117) in front of the proton donor. (*a*) The structure of the present complex 7G shown in a $2F_o - F_c$ map (blue) contoured at 1σ. (*b*) The structure of the native protein (PDB entry 3ur7; grey) shown after superposition on the complex structure, with the glucose residue −1 modelled in the $^4H_3$ conformation (grey). This altered conformation reduces the degree of steric conflict with the side chain of the Glu259 nucleophile, which coincides with a water molecule in the mutant structure.

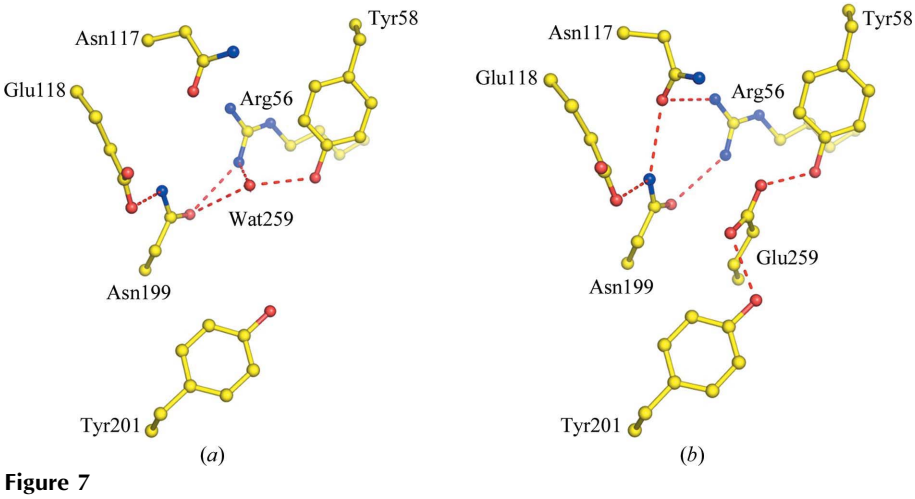

Figure 7
The interaction of the catalytic residues (*a*) in the 7G structure and (*b*) in the native GLUB20-2 structure (PDB entry 3ur7).

flexible part of the protein (Wojtkowiak *et al.*, 2012). Our failure to crystallize a complex with a pentasaccharide may be explained by the insufficient length of the oligosaccharide, which was too short to establish efficient docking interactions; in consequence, the substrate would be unable to properly present the scissile bond to the catalytic centre.

Interestingly, despite the weak interactions of the glucosyl residues at the +1 and +2 subsites of the binding cleft, the histidine tag in the crystal structures (PDB entry 3ur8; Wojtkowiak *et al.*, 2012) of the native protein was bound there (Supplementary Fig. S1[1]). The histidine-tag peptide spanned these two subsites and part of subsite −1, forming hydrogen bonds to the strictly conserved Tyr201 and Glu319 residues.

The kinetic studies reported for the barley enzyme indicated the presence of eight subsites, with the highest binding affinities at subsites −2, +4 and +5, where subsite +5 is located over the subdomain (Hrmova *et al.*, 1995). The glucose residue at the +5 subsite was proposed to interact with the conserved Tyr167. In the present structures (as well as in the native protein models) the side chain of Tyr167 is exposed into the lumen of the catalytic cleft and is not hydrogen-bonded to any other residue, which endows it with high flexibility. It could possibly take part in the association with an extended oligosaccharide chain but, based on the structure and on the lack of evidence for binding of longer (pentameric and hexameric) saccharides there, we do not predict strong binding at this particular subsite.

3.9. Binding-cleft geometry defines substrate specificity of plant endo-1,3-β-glucanases

The long chains of natural (1→3)-β-glucans usually adopt a triple-stranded helical structure with 18 glucose units per pitch: six from each chain (Chuah *et al.*, 1983). In this triple-helical structure, inter-chain hydrogen bonds are formed between three adjacent O-2 hydroxyl groups and intra-chain hydrogen bonds are formed between O-4 hydroxyls and ring O atoms O-5. For comparative studies, a model of a single (1→3)-β-glucan chain was prepared by Bohne *et al.* (1999) using the *SWEET*2 program for constructing three-dimensional models of saccharides from their sequences (Fig. 4*b*). Considered together, the trisaccharide and tetrasaccharide chains bound in the 7G complex form a more linear (less bent) structure, which is achived by a shortening of the O-4···O-5 hydrogen bonds. As illustrated in Fig. 4(*b*), the oligosaccharide in solution modelled by *SWEET*2 has a distinct U-shape and cannot be superposed on the trace of the two oligosaccharide products present in the 7G complex. This suggests that the binding of a substrate molecule prior to the endo-1,3-β-glucanase reaction must involve a substantial deformation at the (−1)–(+1) linkage.

The geometry of the (1→3)-β glycosidic bond defines the specificity of the present enzyme and of other plant endo-1,3-β-glucanases. For example, the cellulose chains with

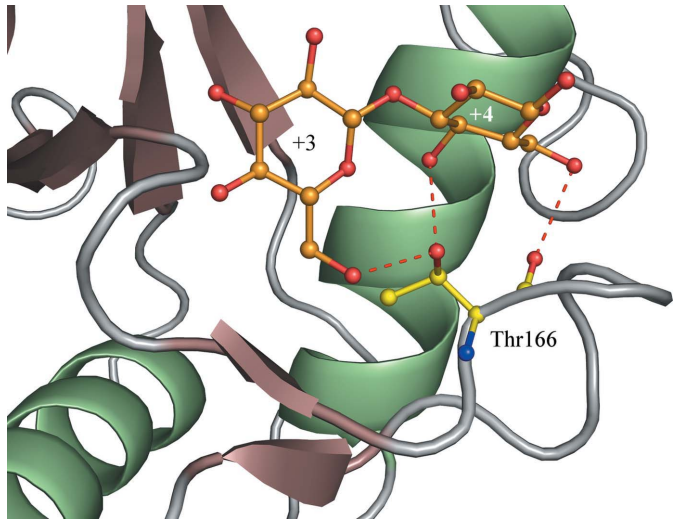

Figure 8
The interactions of units +3 and +4 of the tetrameric (1→3)-β-glucan ligand (orange) with the protein. Hydrogen bonds are marked by dashed lines.

β-1,4-glucosidic linkages are straight and the consecutive glucosyl residues are rotated by 180°, which results in the placement of the O-6 hydroxyls on both sides of the chains. In contrast, the O-6 hydroxyls of 1,3-β-glucans are located on the same side of the oligosaccharide chain. The shape of the substrate-binding cleft of the present protein is not compatible with binding of (1→4)-β-glucans, and β-1,6 branching is only possible at the +1 and +2 subsites (Fig. 9).

The few crystal structures of longer (1→3)-β-oligosaccharides in protein complexes present in the PDB indicate that these oligosaccharides are preferentially recognized in a bent conformation similar to that proposed in solution (Supplementary Fig. S2). For example, the hexasaccharides found in carbohydrate-binding modules are described as 'U-shaped' (Boraston *et al.*, 2002; van Bueren *et al.*, 2005) and the two pentasaccharides present in the catalytic cleft of Gas2p transglycosylase (Hurtado-Guerrero *et al.*, 2009) also adopt such a conformation. The tetrasaccharide found in complex with laminaripentaose-producing β-1,3-glucanase (Wu *et al.*, 2009) was also described as 'forming a distinct kink'.

4. Conclusions

We have presented two crystal structures of the catalytic nucleophile E259A mutant of endo-1,3-β-glucanase from *S. tuberosum* in complexes with products of hexameric (1→3)-β-glucan hydrolysis determined at resolutions of 1.68 and 1.55 Å. Despite the active-site mutation, the protein preparation was still able to convert a laminarahexose hexasaccharide into trisaccharide and tetrasaccharide products, which were found in the crystal structures and the presence of which could be confirmed by mass spectrometry. In the mutated enzyme, the role of the nucleophile could possibly be played by a water molecule accommodated in the space created by the replacement of the longer Glu side chain by

[1] Supplementary material has been deposited in the IUCr electronic archive (Reference: DZ5265). Services for accessing this material are described at the back of the journal.

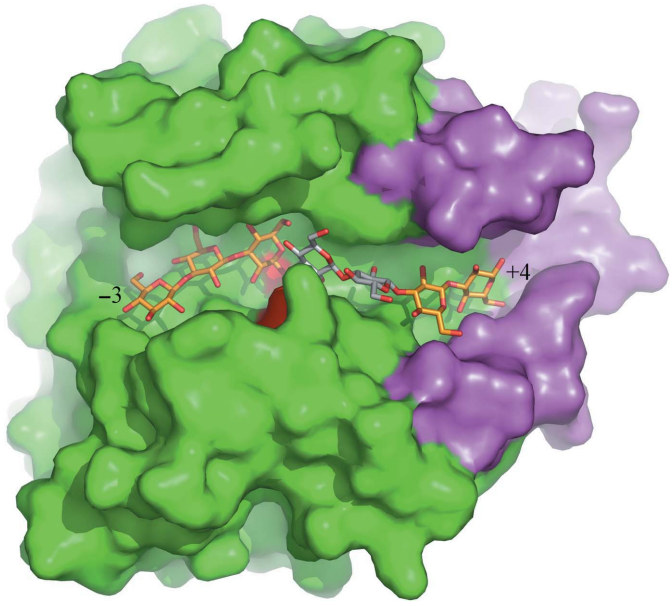

Figure 9
Docking of (1→3)-β-glucans in the binding cleft of plant 1,3-β-glucanase. The protein, viewed from above the TIM barrel looking into the binding cleft, is shown as a green surface representation, except for the proton donor (118) and nucleophilic (259) residues, which are coloured red, and the subdomain region (magenta). The sugar units of the ligands that are included in the crystallographic model (7G) are shown in orange. The two units of the tetrasaccharide ligand that could not be modelled in electron density because of disorder are tentatively marked in this figure in grey (compare with Fig. 4).

Ala. In both structures, the trisaccharide (laminaratriose) occupies the nonreducing end (glycon portion) at subsites −1, −2 and −3 of the binding cleft. At elevated substrate/product concentrations, an additional tetrasaccharide molecule (laminaratetrose) occupies subsites +1, +2, +3 and +4, forming the second complex crystal structure. The tetrasaccharide–enzyme interactions are weak and only two glucose units, found at subsites +3 and +4, are not disordered and could be modelled without ambiguity. The nonreducing terminus of the trisaccharide is placed close to one end of the catalytic cleft delimited by loop $\beta2$–$\alpha2$. The reducing terminal of the tetrasaccharide is placed over the opposite end of the catalytic cleft near helix $\alpha6$. The complexes allow us to dissect in atomic detail the mode in which the polar groups of the oligosaccharides interact with the enzyme in the binding cleft. The trisaccharide units at subsites −1 and −2 interact with residues that are highly conserved among plant 1,3-β-glucanases. In contrast, the glucose units at subsites −3, +3 and +4 interact with variable residues, suggesting different modes of glucose recognition at these sites among different plant endo-1,3-β-glucanases. The geometry of the active-site cleft defines the substrate specificity of the enzyme and excludes the possibility of binding of other oligosaccharide substrates, such as (1→4)-β-glucans, within subsites −3 to +4. Moreover, β-1,6 branching is only possible at subsites +1 and +2. Also, the restricted space at the glycon side of the substrate-binding cleft explains why this plant endo-1,3-β-glucanase has a product profile with a preference for a −3 cleavage. These are the first crystal structures of a plant endo-1,3-β-glucanase representing glycoside hydrolase family GH17 in complex with oligosaccharides.

We wish to thank Dr Jolanta Lukasiewicz and Professor Czeslaw Lugowski (Ludwik Hirszfeld Institute of Immunology and Experimental Therapy, Wroclaw) for help with the mass-spectrometric analyses and Professor Grzegorz Bujacz and Professor Tadeusz Antczak (Technical University of Lodz) for the generous gift of homogenous (1→3)-β-glucans.

References

Akiyama, T., Shibuya, N., Hrmova, M. & Fincher, G. B. (1997). *Carbohydr. Res.* **297**, 365–374.
Bohne, A., Lang, E. & von der Lieth, C. W. (1999). *Bioinformatics*, **15**, 767–768.
Boraston, A. B., Nurizzo, D., Notenboom, V., Ducros, V., Rose, D. R., Kilburn, D. G. & Davies, G. J. (2002). *J. Mol. Biol.* **319**, 1143–1156.
Bueren, A. L. van, Morland, C., Gilbert, H. J. & Boraston, A. B. (2005). *J. Biol. Chem.* **280**, 530–537.
Cantarel, B. L., Coutinho, P. M., Rancurel, C., Bernard, T., Lombard, V. & Henrissat, B. (2009). *Nucleic Acids Res.* **37**, D233–D238.
Chen, L., Garrett, T. P., Fincher, G. B. & Høj, P. B. (1995). *J. Biol. Chem.* **270**, 8093–8101.
Chuah, C. T., Sarko, A., Deslandes, Y. & Marchessault, R. H. (1983). *Macromolecules*, **16**, 1375–1382.
Cohen, G. H. (1997). *J. Appl. Cryst.* **30**, 1160–1161.
Davies, G. J., MacKenzie, L., Varrot, A., Dauter, M., Brzozowski, A. M., Schülein, M. & Withers, S. G. (1998). *Biochemistry*, **37**, 11707–11713.
Davies, G. J., Planas, A. & Rovira, C. (2012). *Acc. Chem. Res.* **45**, 308–316.
Davies, G. J., Wilson, K. S. & Henrissat, B. (1997). *Biochem. J.* **321**, 557–559.
Fibriansah, G., Masuda, S., Koizumi, N., Nakamura, S. & Kumasaka, T. (2007). *Proteins*, **69**, 683–690.
Green, M. R. & Sambrook, P. (2012). *Molecular Cloning: A Laboratory Manual*, 4th ed. Cold Spring Harbor Laboratory Press.
Henrissat, B., Callebaut, I., Fabrega, S., Lehn, P., Mornon, J. P. & Davies, G. (1995). *Proc. Natl Acad. Sci. USA*, **92**, 7090–7094.
Hrmova, M. & Fincher, G. B. (1993). *Biochem. J.* **289**, 453–461.
Hrmova, M., Garrett, T. P. & Fincher, G. B. (1995). *J. Biol. Chem.* **270**, 14556–14563.
Hrmova, M., Imai, T., Rutten, S. J., Fairweather, J. K., Pelosi, L., Bulone, V., Driguez, H. & Fincher, G. B. (2002). *J. Biol. Chem.* **277**, 30102–30111.
Huecas, S., Villalba, M. & Rodríguez, R. (2001). *J. Biol. Chem.* **276**, 27959–27966.
Hurtado-Guerrero, R., Schüttelkopf, A. W., Mouyna, I., Ibrahim, A. F., Shepherd, S., Fontaine, T., Latgé, J.-P. & van Aalten, D. M. F. (2009). *J. Biol. Chem.* **284**, 8461–8469.
Ishida, T., Fushinobu, S., Kawai, R., Kitaoka, M., Igarashi, K. & Samejima, M. (2009). *J. Biol. Chem.* **284**, 10100–10109.
Jenkins, J., Lo Leggio, L., Harris, G. & Pickersgill, R. (1995). *FEBS Lett.* **362**, 281–285.
Keen, N. T. & Yoshikawa, M. (1983). *Plant Physiol.* **71**, 460–465.
Laughrea, M., Latulippe, J., Filion, A.-M. & Boulet, L. (1987). *Eur. J. Biochem.* **169**, 59–64.
Loon, L. C. van, Pierpoint, W. S., Boller, T. & Conejero, V. (1994). *Plant Mol. Biol. Rep.* **12**, 245–264.
McNaught, A. D. & Wilkinson, A. (1997). *IUPAC Compendium of Chemical Terminology*, 2nd ed. Oxford: Blackwell Scientific Publications.
McRee, D. E. (1999). *J. Struct. Biol.* **125**, 156–165.

Moore, A. E. & Stone, B. A. (1972). *Biochim. Biophys. Acta*, **258**, 248–264.
Murshudov, G. N., Skubák, P., Lebedev, A. A., Pannu, N. S., Steiner, R. A., Nicholls, R. A., Winn, M. D., Long, F. & Vagin, A. A. (2011). *Acta Cryst.* D**67**, 355–367.
Otwinowski, Z. & Minor, W. (1997). *Methods Enzymol.* **276**, 307–326.
Painter, J. & Merritt, E. A. (2006). *J. Appl. Cryst.* **39**, 109–111.
Peumans, W. J., Barre, A., Derycke, V., Rougé, P., Zhang, W., May, G. D., Delcour, J. A., Van Leuven, F. & Van Damme, E. J. (2000). *Eur. J. Biochem.* **267**, 1188–1195.
Schüttelkopf, A. W. & van Aalten, D. M. F. (2004). *Acta Cryst.* D**60**, 1355–1363.
Studier, F. W. & Moffatt, B. A. (1986). *J. Mol. Biol.* **189**, 113–130.
Sunderasan, E., Hamzah, S., Hamid, S., Ward, M. A., Yeang, H. Y. & Cardosa, M. J. (1995). *J. Nat. Rubb. Res.* **10**, 82–99.
Toth, M. J., Murgola, E. J. & Schimmel, P. (1988). *J. Mol. Biol.* **201**, 451–454.
Vagin, A. & Teplyakov, A. (2010). *Acta Cryst.* D**66**, 22–25.
Varghese, J. N., Garrett, T. P., Colman, P. M., Chen, L., Høj, P. B. & Fincher, G. B. (1994). *Proc. Natl Acad. Sci. USA*, **91**, 2785–2789.
Vocadlo, D. J. & Davies, G. J. (2008). *Curr. Opin. Chem. Biol.* **12**, 539–555.
Wagner, S., Radauer, C., Hafner, C., Fuchs, H., Jensen-Jarolim, E., Wüthrich, B., Scheiner, O. & Breiteneder, H. (2004). *Clin. Exp. Allergy*, **34**, 1739–1746.
Watson, J. N., Dookhun, V., Borgford, T. J. & Bennet, A. J. (2003). *Biochemistry*, **42**, 12682–12690.
Witek, A. I., Witek, K. & Hennig, J. (2008). *Acta Biochim. Pol.* **55**, 791–797.
Wojtkowiak, A., Witek, K., Hennig, J. & Jaskolski, M. (2012). *Acta Cryst.* D**68**, 713–723.
Wu, H.-M., Liu, S.-W., Hsu, M.-T., Hung, C.-L., Lai, C.-C., Cheng, W.-C., Wang, H.-J., Li, Y.-K. & Wang, W.-C. (2009). *J. Biol. Chem.* **284**, 26708–26715.
Zechel, D. L. & Withers, S. G. (2001). *Curr. Opin. Chem. Biol.* **5**, 643–649.